ACS Catalysis

RESEARCH ARTICLE

pubs.acs.org/acscatalysis

Zeolite- and MgO-Supported Molecular Iridium Complexes: Support and Ligand Effects in Catalysis of Ethene Hydrogenation and H−D Exchange in the Conversion of $H_2 + D_2$

Jing Lu, Pedro Serna, and Bruce C. Gates*

Department of Chemical Engineering and Materials Science, University of California, Davis, One Shields Avenue, Davis, California 95616, United States

Supporting Information

ABSTRACT: Zeolite- and MgO-supported mononuclear iridium diethene complexes were formed by the reaction of $Ir(C_2H_4)_2(acac)$ (acac = acetylacetonate, $C_5H_7O_2^-$) with each support. Changes in the ligand environment of the supported iridium complexes were characterized by infrared, X-ray absorption near edge structure, and extended X-ray absorption fine structure spectroscopies as various mixtures of H_2, C_2H_4, and CO flowed over the samples. In contrast to the nonuniform metal complexes anchored to metal oxides, our zeolite-supported metal complexes were highly uniform, allowing precise determinations of the chemistry, including the role of the support as a macroligand. Zeolite- and MgO-supported $Ir(C_2H_4)_2$ complexes are each rapidly converted to $Ir(CO)_2$ upon contact with a pulse of CO, and the ν_{CO} frequencies indicate that the iridium is more electron-deficient when the support is the zeolite. The $Ir(CO)_2$ complex supported on MgO was highly stable in the presence of various combinations of CO, C_2H_4, and helium. In contrast, the zeolite-supported $Ir(CO)_2$ complex was found to be highly reactive, forming $Ir(CO)_3$, $Ir(CO)(C_2H_4)$, $Ir(CO)_2(C_2H_4)$, and $Ir(CO)(C_2H_4)_2$. The π-bonded ethene ligands of the zeolite-supported $Ir(C_2H_4)_2$ in H_2 were facilely converted to σ-bonded ethyl when treated. However, the stability of the ethene ligands was markedly increased when the support was changed to MgO or when a CO ligand was simultaneously bonded to the iridium. The rates of catalytic ethene hydrogenation and H_2/D_2 exchange in the presence of a catalyst initially consisting of $Ir(C_2H_4)_2$ on the zeolite were found to be more than an order of magnitude higher than when MgO was the support. The iridium complexes containing one or more CO ligands were found to be inactive for H_2/D_2 exchange reactions when the support was MgO, but they were moderately active when it was the zeolite. The effects of the MgO and zeolite supports on reactivity and catalytic activity are attributed to their differences as ligands donating or withdrawing electrons, respectively.

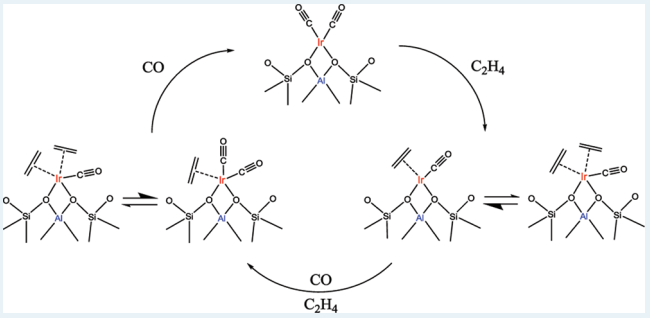

KEYWORDS: supported iridium complex catalyst, zeolite, MgO, ethene hydrogenation, IR spectroscopy, EXAFS spectroscopy

INTRODUCTION

Supported metal catalysts, which are used widely in industrial processes, consist of metal species dispersed on porous supports, usually metal oxides or zeolites. The metal species range from single metal atoms (usually cations), to metal clusters consisting of a few atoms each, to metal nanoparticles that are large enough to have the character of bulk metals. The performance of a supported catalyst is influenced by the composition and structure of the metal species, the ligands bonded to the metal, and the support. The smaller the metal species, the greater are the effects of the ligands and the support, which itself may be considered a ligand. In contrast, when the supported species are particles large enough to have bulklike properties, the support effect may be negligible.[1]

Typical supported metal catalysts are highly complex and nonuniform structurally, and the nonuniformity characterizes both the metal species and the support surfaces. Opportunities for maximizing the role of the support and understanding it better are optimal when the uniformity of the catalyst is maximized: thus, when all the catalytically active sites are equivalent and bonded to a support that is uniform (crystalline).[2,3] Opportunities for understanding support effects are further optimized when the catalytic species are mononuclear metal complexes with a substantial number of bonds to the support.

Our goals were to gain understanding of the catalytic properties of supported iridium complex catalysts by using spectroscopic methods to track the reactions of the complexes with small ligands introduced into the sample from the gas phase, with these ligands being chosen to include those involved in catalytic reactions of ethene and H_2. Thus, we sought fundamental understanding

Received: August 4, 2011
Revised: September 15, 2011
Published: September 26, 2011

Table 1. Summary of Spectroscopic and Catalytic Test Results with Proposed Structures of DAY Zeolite- and MgO-Supported Iridium Complexes[a]

	EXAFS parameters						supported iridium species			
sample/treatment conditions	absorber−backscatterer pair	N	R (Å)	$10^3 \times \Delta\sigma^2$ (Å^2)	ΔE_0 (eV)	IR bands in the ν_{CO} region of supported species (cm^{-1})	major	minor	TOF for ethene hydrogenation (s^{-1})	activity for H_2/D_2 exchange (% conversion)
zeolite-supported $Ir(C_2H_4)_2$ in helium at 300 K	Ir−$O_{zeolite}$	2.0	2.12	13	−5.1					
	Ir−C_{ethene}	4.1	2.10	10	−2.2	*b*	$Ir(C_2H_4)_2$	*c*		
	Ir−Al	1.1	3.02	6.8	−7.9					
zeolite-supported $Ir(C_2H_4)_2$ after 20 min in H_2 at 300 K	Ir−$O_{zeolite}$	1.9	2.11	7.2	−2.6					
	Ir−C_{ethene}	1.8	2.02	10	−2.7	*b*	$Ir(C_2H_5)_2$	*c*	0.69	11
	Ir−Al	1.1	2.98	5.4	−8.0					
	Ir−C_{long}	1.7	3.20	5.0	0.20					
zeolite-supported $Ir(C_2H_4)_2$ treated with a pulse of CO in helium at 300 K	Ir−$O_{zeolite}$	2.1	2.11	2.1	5.4					
	Ir−C_{CO}	2.0	1.85	3.6	−2.3	2038, 2109	$Ir(CO)_2$	*c*		0.51
	Ir−O_{CO}	2.0	2.99	2.4	−9.9					
	Ir−Al	1.1	2.87	1.1	4.3					
zeolite-supported $Ir(CO)_2$ treated in C_2H_4 at 300 K	Ir−$O_{zeolite}$ and Ir−C_{ethene}	5.0	2.21	7.1	−5.8					
	Ir−C_{CO}	1.1	1.90	4.1	−5.5	2054, 2087	$Ir(CO)(C_2H_4)$	$Ir(CO)(C_2H_4)_2$	0	0.27
	Ir−O_{CO}	1.1	3.05	1.9	−8.0					
	Ir−Al	1.0	2.91	1.9	6.5					
zeolite-supported $Ir(CO)_2$ treated in C_2H_4 at 393 K	Ir−$O_{zeolite}$ and Ir−C_{ethene}	3.9	2.25	4.5	−7.8					
	Ir−C_{CO}	0.9	2.12	1.3	8.0	2054	$Ir(CO)(C_2H_4)$	*c*		
	Ir−O_{CO}	0.9	2.94	5.6	−3.6					
	Ir−Al	1.1	3.02	9.9	1.1					
zeolite-supported $Ir(CO)_2$ treated in C_2H_4 followed by purging with helium at 300 K	Ir−$O_{zeolite}$ and Ir−C_{ethene}	3.6	2.13	8.8	−8.0					
	Ir−C_{CO}	1.3	1.85	9.3	2.0	2054, 2038, 2109	$Ir(CO)(C_2H_4)$	$Ir(CO)_2$		0.63
	Ir−O_{CO}	1.3	2.97	14	−6.3					
	Ir−Al	1.1	3.01	5.6	−8.0					
zeolite-supported $Ir(CO)_2$ treated in CO and C_2H_4 at 300 K	Ir−$O_{zeolite}$ and Ir−C_{ethene}	4.3	2.05	11	8.0					
	Ir−C_{CO}	1.8	1.89	5.5	−8.0	2087, 2111	$Ir(CO)_2(C_2H_4)$	$Ir(CO)(C_2H_4)_2$	0	0
	Ir−O_{CO}	1.8	2.94	8.9	−5.0					
	Ir−Al	1.2	3.09	0.8	3.8					
MgO-supported $Ir(C_2H_4)_2$ in He at 300 K	Ir−O_{MgO}	2.1	2.01	5.8	−7.4					
	Ir−C_{ethene}	4.1	2.13	6.0	−6.2	*b*	$Ir(C_2H_4)_2$	*c*	0.03	0.72
	Ir−Mg	1.5	3.06	9.4	−5.0					
MgO-supported $Ir(C_2H_4)_2$ after 2 h in H_2 flow at 300 K	Ir−O_{MgO}	1.9	2.12	3.9	−3.4					
	Ir−C_{ethene}	3.6	2.06	6.1	−8.0	*b*	$Ir(C_2H_4)_2$	*c*	0.03	0.72
	Ir−Mg	2.5	2.98	11	0.35					
	Ir−O_{long}	4.1	3.66	9.0	−4.7					

dx.doi.org/10.1021/cs200397r |*ACS Catal.* 2011, 1, 1549–1561

Table 1. Continued

sample/treatment conditions	EXAFS parameters: absorber–backscatterer pair	N	R (Å)	$10^3 \times \Delta\sigma^2$ (Å^2)	ΔE_0 (eV)	IR bands in the ν_{CO} region of supported species (cm^{-1})	supported iridium species: major	supported iridium species: minor	TOF for ethene hydrogenation (s^{-1})	activity for H_2/D_2 exchange (% conversion)
MgO-supported $Ir(C_2H_4)_2$ treated with a pulse of CO in He at 300 K	Ir−O_{MgO}	1.9	2.05	3.7	−3.2					
	Ir−C_{CO}	1.9	1.83	9.5	4.2					
	Ir−O_{CO}	1.9	3.00	4.6	−8.0	1967, 2051	$Ir(CO)_2$	[c]	0	0
	Ir−Mg	1.6	2.89	8.0	4.5					
MgO-supported $Ir(CO)_2$ treated in C_2H_4 at 300 K	Ir−O_{MgO}	1.9	2.04	3.8	1.1					
	Ir−C_{CO}	1.8	1.89	7.9	−3.1					
	Ir−O_{CO}	1.8	3.00	5.6	−8.0	1967, 2051	$Ir(CO)_2$	[c]	0	0
	Ir−Mg	1.5	2.93	9.3	3.0					

[a] Notation: N, coordination number; R, distance between absorber and backscatterer atoms; $\Delta\sigma^2$, variance in the absorber−backscatterer distance; ΔE_0, inner potential correction. Error bounds (accuracies) characterizing the structural parameters, obtained by EXAFS spectroscopy are estimated to be as follows: N, ±20%; R, ±0.02 Å; $\Delta\sigma^2$, ±20%; and ΔE_0, ±20%. [b] No IR bands in this region. [c] No minor species exist at this condition.

of the organometallic and catalytic chemistry and, specifically, the ligand effects. All the experiments were performed with gas-phase reactants to eliminate the possibility of the complicating solvent effects that can occur in homogeneous catalysis.

The iridium complexes, on the acidic support dealuminated HY zeolite (DAY zeolite) or the basic support MgO, were synthesized to incorporate initially reactive ethene ligands[4] and then exposed in flow reactors to gas-phase compounds that modified the ligand sphere of the iridium. H_2, D_2, CO, and C_2H_4 were the gas-phase compounds; ethene hydrogenation and H-D exchange (in the reaction of H_2 with D_2) were the catalytic reactions, and IR and X-ray absorption spectroscopies were the characterization methods.

The results demonstrate the essential role of the support as a ligand that, in combination with other ligands, affects the reactivity of the metal species and their catalytic behavior in reactions of H_2 and ethene. The data indicate an opportunity to tune the properties of supported metal complex catalysts by choice of electron-withdrawing or -donating supports.

RESULTS

Structural Characterization of Initially Prepared Zeolite- and MgO-Supported Iridium Complexes. IR spectra characterizing the samples prepared by reaction of $Ir(C_2H_4)_2(acac)$ (acac is acetylacetonate) with the surfaces of DAY zeolite and highly dehydroxylated MgO indicate that the iridium complexes retained the ethene ligands upon adsorption, as expected,[4,5] and as confirmed by the presence of bands at 3001 and 3032 cm^{-1} (when the support was MgO) and 3022 and 3082 cm^{-1} (when it was the zeolite). These bands are assigned to ν_{CH} stretching vibrations of ethene π-bonded to isolated Ir atoms (Figure S1 of the Supporting Information), approximately matching those of the $Ir(C_2H_4)_2(acac)$ precursor.[4,6] Consistent with these results, the IR spectra show that the acac ligands were completely removed from the iridium when $Ir(C_2H_4)_2(acac)$ was adsorbed (Figures S5 and S6 of the Supporting Information). We suggest that the removal of acac ligands led to the formation of Hacac in the reaction with H^+ of the AlOH sites of the zeolite or MgOH site of the MgO (or it could have led to the formation of Mg(acac) on MgO at O vacancies on MgO).[7] Spectra are shown in the Supporting Information.

In agreement with the IR data, extended X-ray absorption fine structure (EXAFS) data characterizing the species formed from $Ir(C_2H_4)_2(acac)$ on each support (Table 1) indicate that each Ir atom was bonded, on average, to two ethene ligands (the Ir−C coordination number was nearly 4, with a bonding distance of 2.10 Å) and to two support O atoms (the Ir−O coordination number was nearly 2, with a bonding distance of 2.12 Å). The EXAFS data (Tables S2 and S3 of the Supporting Information) show that the iridium complexes were bonded near several magnesium sites on MgO (and likely were bonded to the support surface at more than one type of binding site, such as defects), whereas they were evidently bonded at single and nearly equivalent aluminum sites on the zeolite support, as expected.[4,8] Moreover, no Ir−Ir contributions were detected, consistent with the lack of iridium clusters.

Reaction of Supported Iridium Diethene Complexes with CO. When each of the supported iridium diethene complexes was treated with a pulse of 10% CO in helium flowing at 300 K and 1 bar (the pressure applied in all the gas treatments), a rapid replacement of the C_2H_4 ligands by CO took place (Figure 1), as

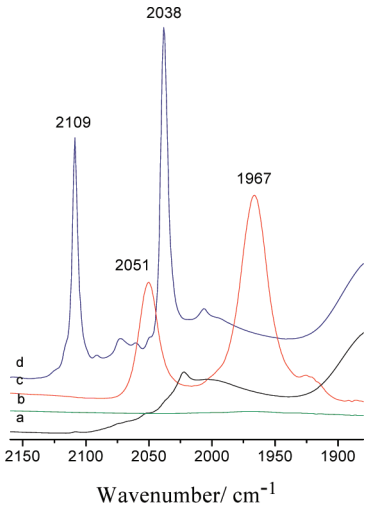

Figure 1. IR spectra (absorbance) in the ν_{CO} region characterizing supported iridium complexes: (a) initially prepared $Ir(C_2H_4)_2$ on DAY zeolite; (b) initially prepared $Ir(C_2H_4)_2$ on MgO; (c) sample formed by treatment of $Ir(C_2H_4)_2$ on MgO with a 20-mL pulse of 10% CO in helium; (d) sample formed from $Ir(C_2H_4)_2$ on DAY zeolite treated with a 20-mL pulse of 10% CO in helium.

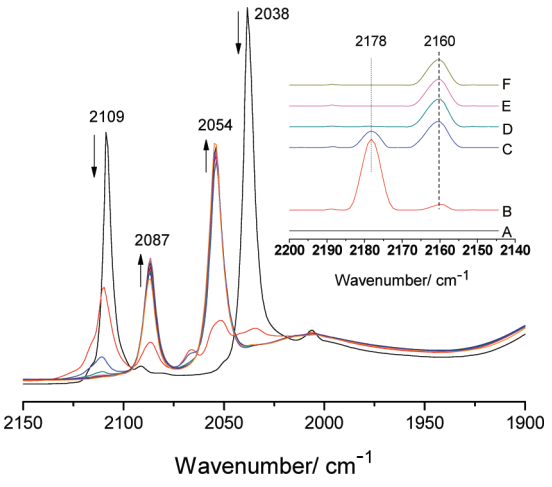

Figure 2. IR spectra (absorbance) in the ν_{CO} region characterizing changes in the sample initially consisting of $Ir(CO)_2$ on DAY zeolite as it was exposed to flowing C_2H_4 at 300 K for 10 min. The inset represents the CO stretching region characterizing CO interacting with hydroxyl groups on the zeolite surface after the start of C_2H_4 flow for the following periods (min): (A) 0, (B) 1, (C) 2, (D) 3, (E) 4, and (F) 5. The arrows indicate the directional changes in absorbance of individual peaks as a function of time. (Complementary data collected with $Ir(^{13}CO)_2$ are shown in the Supporting Information.).

shown by the disappearance of IR bands at 3001 and 3032 cm^{-1} when the support was MgO and at 3022 and 3082 cm^{-1} when the support was the zeolite. There was a concomitant growth of new bands at 1967 and 2051 cm^{-1} (with the MgO support) and at 2038 and 2109 cm^{-1} (with the zeolite), indicating the formation of iridium *gem*-dicarbonyls.[9−11] The replacement of ethene by CO was complete within 2 min, consistent with earlier observations[4,12−14] and with the following schematic depiction (where the braces denote O atoms that are part of the support surface):

$$Ir(C_2H_4)_2\{O_2\} + 2CO \rightarrow Ir(CO)_2\{O_2\} + 2C_2H_4 \quad (1)$$

The IR ν_{CO} bands of $Ir(CO)_2$ complexes supported on the zeolite, each having a full width at half-maximum (fwhm) of ~5 cm^{-1}, are sharper than those assigned to the isostructural species on MgO (fwhm ≈ 25 cm^{-1}). The sharp bands indicate a higher degree of uniformity of the species on the zeolite,[15] corresponding to the well-defined crystalline structure of this support and the fact that bonding of the iridium to its surface takes place specifically at Al^- sites. Moreover, the high degree of site isolation of the Al^- sites on the zeolite in comparison with the Mg sites on MgO led to greater uniformity of the isolated iridium species on the zeolite.

The IR results were confirmed by EXAFS spectra taken at the Ir L_{III} edge for the MgO- and zeolite-supported $Ir(C_2H_4)_2$ complexes treated with 10% CO (in helium) for 30 s at 300 K. The spectra indicate changes in the ligand environment of iridium, characterized by the disappearance of the $Ir-C_{ethene}$ contributions and the appearance of new contributions assigned to $Ir-C_{CO}$ and to $Ir-O_{CO}$ (Table 1). The EXAFS data indicate multiple scattering paths characteristic of linear Ir−C−O moieties, and the $Ir-C_{CO}$ and $Ir-O_{CO}$ distances confirm the presence of terminally bonded CO ligands (Table 1). The $Ir-C_{CO}$ and $Ir-O_{CO}$ coordination numbers of nearly 2 and the lack of EXAFS evidence of iridium clusters demonstrate the presence of mononuclear iridium *gem*-dicarbonyls on each support, in agreement with the IR spectra.

Additional IR experiments were performed with the supported $Ir(C_2H_4)_2$ complexes in continuously flowing 10% CO in helium at 300 K. The spectrum of the MgO-supported iridium complex indicated the appearance of the pair of bands, at 1967 and 2051 cm^{-1}, assigned to iridium *gem*-dicarbonyls (CO in the gas phase was also observed). When the support was the zeolite, new bands formed at 2073 and 2098 cm^{-1}, in addition to those at 2038 and 2109 cm^{-1} assigned to $Ir(CO)_2$ species (SI Figure S9). These new bands at 2073 and 2098 cm^{-1} disappeared after switching of the gas stream to helium, with reversible formation of $Ir(CO)_2$ as the only surface species.

Reaction of Supported Iridium Dicarbonyl Complexes with C_2H_4. When the MgO-supported iridium dicarbonyl complexes were treated in flowing C_2H_4 at 300 K, the ν_{CO} bands at 1967 and 2051 cm^{-1} remained intact, even after 2 h (SI Figure S2). Nor was any change observed after this treatment in the ν_{CH} region of the spectrum after C_2H_4 had been purged from the gas phase with helium (SI Figure S1), indicating that the alkene did not become bonded to the iridium.

In agreement with the IR results, when the MgO-supported iridium dicarbonyl complexes were treated in flowing C_2H_4 in the EXAFS cell, no changes in the iridium ligation were detected (Table 1); the Fourier transform of the EXAFS data is almost identical to that observed before the start of C_2H_4 flow, corresponding to the presence of just the $Ir(CO)_2$ species on MgO (SI Figures S23 and S24).

In contrast, when the sample was the zeolite-supported $Ir(CO)_2$, exposure to flowing C_2H_4 at 300 K led to changes in both the IR and EXAFS spectra, as follows: The initial ν_{CO} bands at 2038 and 2109 cm^{-1} disappeared within 3 min, with the simultaneous growth of new bands at 2054 and 2087 cm^{-1} (Figure 2). Two additional weak bands, at 2160 and 2178 cm^{-1}, also appeared in the ν_{CO} region (Figure 2 inset); the band at 2178 cm^{-1} formed immediately after the start of C_2H_4 flow and gradually disappeared in the next 4 min as the band at 2160 cm^{-1} grew. Complementing

dx.doi.org/10.1021/cs200397r |ACS Catal. 2011, 1, 1549–1561

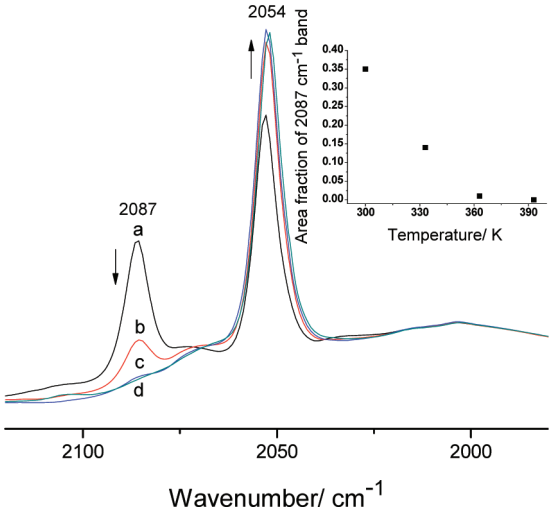

Figure 3. IR spectra (absorbance) in the ν_{CO} region characterizing changes in the sample consisting initially of DAY zeolite-supported $Ir(CO)_2$ as it was treated in flowing C_2H_4, after reaching steady state at each of the following temperatures (K): (a) 300, (b) 333, (c) 363, and (d) 393. The inset represents the fraction of peak area under the peak at ν = 2087 cm^{-1} relative to total area under both peaks as a function of temperature. The arrows indicate the directional change of absorbance of individual peaks as a function of time.

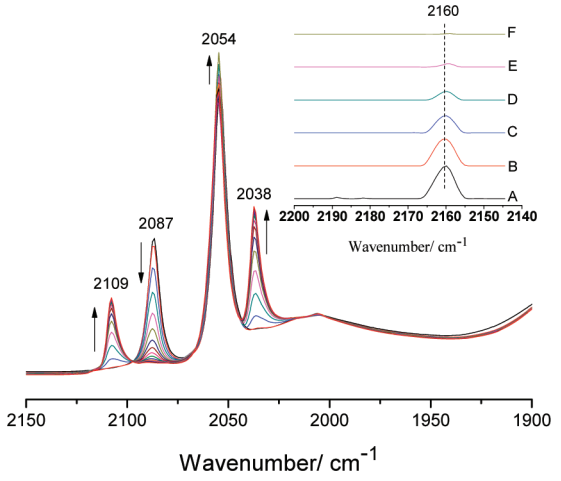

Figure 4. IR spectra (absorbance) in the ν_{CO} region characterizing the sample initially consisting of $Ir(CO)_2$ on DAY zeolite purged with helium at 300 K, after treatment in a continuous flow of C_2H_4, over a period of 15 min. The inset represents the CO stretching region characterizing CO interacting with hydroxyl groups on the zeolite surface after the start of helium flow for the following times (min): (A) 0, (B) 1, (C) 2, (D) 3, (E) 4, and (F) 5. The arrows indicate the directional changes of absorbance of the individual peaks as a function of time. (Data collected with $Ir(^{13}CO)_2$ are shown in the Supporting Information.).

these results, EXAFS data (Table 1) show that the $Ir-C_{CO}$ and $Ir-O_{CO}$ coordination numbers decreased from ~2 to ~1, indicating the removal of one of the initial two CO ligands of the complex. Concomitantly, the coordination number corresponding to the contributions at short Ir−backscatterer distances (characterizing the sum of $Ir-O_{zeolite}$ + $Ir-C_{ethene}$)[16] increased from 2.1 to 5.0 (Table 1). These data point to the replacement of one of the carbonyl ligands with a hydrocarbon, presumably ethene.

Indeed, purging of the gas-phase ethene from the cell with helium enabled a straightforward analysis of the ν_{CH} stretching vibrations characterizing the supported species. Thus, bands at 3023 and 3078 cm^{-1} were observed after the treatment of the zeolite-supported $Ir(CO)_2$ complexes with C_2H_4, indicating the presence of ethene π-bonded to the iridium (Figure S1). Evidently, after sufficient exposure of the sample to ethene, ethene partially displaced the tightly bonded CO from the iridium.

Additional experiments were performed with the zeolite-supported $Ir(CO)_2$ complexes in flowing C_2H_4 as the treatment temperature was ramped up. The IR spectra show that the 2087-cm^{-1} band decreased in intensity as the temperature was raised from 300 to 393 K, disappearing when it reached about 393 K (at each temperature, a 5-min hold allowed the spectrum to reach steady state). Concurrently, the intensity of the 2054-cm^{-1} band increased, reaching a maximum at the highest temperature (Figure 3). These changes were also characterized by EXAFS spectroscopy. When the temperature increased to 393 K, the $Ir-C_{CO}$ and $Ir-O_{CO}$ contributions remained essentially unchanged, with coordination numbers of ~2, while the coordination numbers characterizing the Ir−backscatterer contributions at relatively short distances decreased from 5.0 to 3.9 (Table 1). These spectra show that, on average, the number of CO ligands in the iridium complex remained unchanged while the number of hydrocarbon ligands decreased.

The changes in the zeolite-supported iridium complexes were also characterized with the sample in flowing helium after treatment with flowing C_2H_4 at 300 K. As the intensity of the IR band at 2054 cm^{-1} increased with the sample in helium, the band at 2087 cm^{-1} decreased sharply, disappearing after 15 min (Figure 4). Simultaneously, partial recovery of the bands indicative of iridium dicarbonyls, at 2038 and 2109 cm^{-1}, was accompanied by a decrease in the intensity of the band at 2160 cm^{-1}, which disappeared after 5 min.

After the C_2H_4 flow had been stopped and the cell had been purged with helium for 30 min at 300 K, EXAFS data recorded with the sample in flowing helium showed a slight increase in the coordination numbers characterizing the $Ir-C_{CO}$ and $Ir-O_{CO}$ contributions, from 1.1 to 1.3, which is consistent with the IR data suggests that once the gas-phase ethene was removed, recarbonylation of a small fraction of the iridium complexes occurred, forming $Ir(CO)_2$. There was also a significant decrease (from 5.0 to 3.6) in the coordination number of the Ir−backscatterer contributions at a short distance (Table 1), indicating the loss of hydrocarbon ligands from the iridium.

Reaction of Zeolite-Supported Iridium Dicarbonyl Complexes with Mixtures of C_2H_4 and CO. When a stream of C_2H_4 and CO (2:1 molar ratio) was brought into contact with the zeolite-supported $Ir(CO)_2$ at 300 K, the ν_{CO} IR spectra changed rapidly, in contrast to what was observed with the isostructural species on MgO, which remained unchanged. The peaks at 2038 and 2109 cm^{-1} representing $Ir(CO)_2$ on the zeolite disappeared immediately, just as a sharp peak at 2087 cm^{-1} and a broader band centered at ~2111 cm^{-1} appeared (Figure 5). EXAFS spectra characterizing the initial zeolite-supported $Ir(CO)_2$ in the presence of C_2H_4 + CO showed a slight decrease in the coordination numbers of the $Ir-C_{CO}$ and $Ir-O_{CO}$ contributions (each from 2 to 1.8), indicating that the iridium complexes were still bonded to approximately two CO ligands, on average, whereas the coordination number characterizing the Ir−backscatterer

dx.doi.org/10.1021/cs200397r |ACS Catal. 2011, 1, 1549–1561

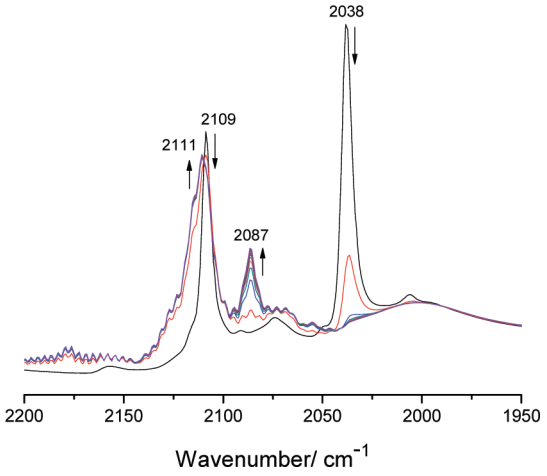

Figure 5. IR spectra (absorbance) in the ν_{CO} region characterizing the sample initially consisting of DAY zeolite-supported $Ir(CO)_2$ as it was treated in flowing CO + C_2H_4 at 300 K. The spectra were recorded for 30 min after the start of flow of CO + C_2H_4. The arrows indicate the directional changes of absorbance of individual peaks as a function of time.

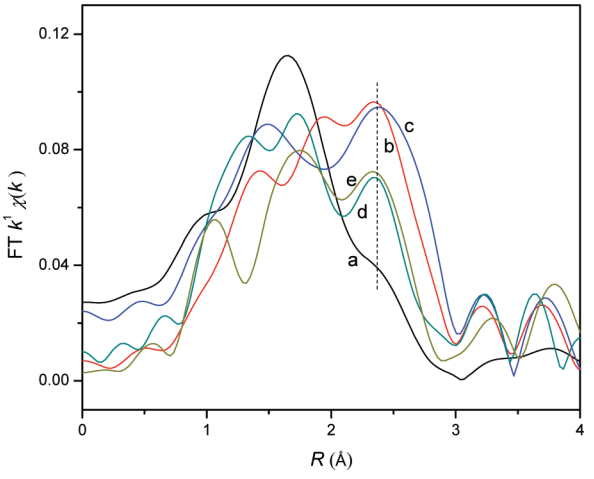

Figure 6. k^1-Weighted uncorrected magnitudes of the Fourier transforms of the EXAFS data recorded at the Ir L_{III}-edge characterizing DAY zeolite-supported iridium complexes under the following treatment conditions: (a) $Ir(C_2H_4)_2$ in helium, (b) $Ir(CO)_2$ prepared by treating supported $Ir(C_2H_4)_2$ with a 20-mL pulse of CO in helium, (c) sample formed from supported $Ir(CO)_2$ in CO + C_2H_4, (d) sample formed from supported $Ir(CO)_2$ in C_2H_4, and (e) sample formed from supported $Ir(CO)_2$ treated in C_2H_4 followed by purging with helium.

contribution at a short distance increased from 2.1 to 4.3, suggesting that although no significant decarbonylation occurred, additional hydrocarbon ligands (presumably ethene) became bonded to the iridium.

X-ray Absorption Spectra of the MgO- and Zeolite-Supported Samples. The Fourier transformed EXAFS spectra and X-ray absorption near edge structure (XANES) spectra of the zeolite-supported iridium complexes under the conditions mentioned above are shown in Figures 6 and 7. The interpretations of these spectra and comparisons with IR results are presented in the Discussion section.

Reaction of Supported Iridium Diethene Complexes with H_2. IR spectra characterizing the zeolite-supported $Ir(C_2H_4)_2$

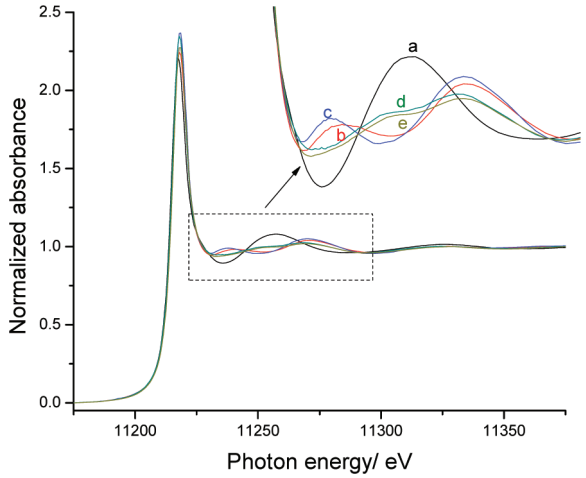

Figure 7. XANES spectra at the Ir L_{III}-edge characterizing DAY zeolite-supported iridium complexes under the following treatment conditions: (a) $Ir(C_2H_4)_2$ in helium, (b) $Ir(CO)_2$ prepared by treating $Ir(C_2H_4)_2$ with a 20-mL pulse of CO in helium, (c) sample formed from $Ir(CO)_2$ in CO + C_2H_4, (d) sample formed from $Ir(CO)_2$ in C_2H_4, and (e) sample formed from $Ir(CO)_2$ treated with C_2H_4 followed by purging with helium.

complexes in flowing H_2 at 300 K (Figure S3) show that the bands initially observed at 3022 and 3082 cm^{-1}, characterizing ethene ligands on iridium, disappeared within 5 min of contact with H_2, and, at the same time, bands grew in at 2964, 2936, 2876, and 2854 cm^{-1}, characterizing σ-bonded hydrocarbon ligands (Figure S7).

This result provides a sharp contrast with the reactivity of the iridium ethene complexes on MgO, as the initial π-bonded ethene ligands were found to be highly stable in H_2 at 300 K, with the bands at 3001 and 3032 cm^{-1} ascribed to the ν_{CH} stretching vibration of the C═C bond undergoing only a slight decrease in intensity after 3 h of contact with H_2 (Figure S3).

In agreement with the IR results, EXAFS data show that when the zeolite-supported $Ir(C_2H_4)_2$ was treated in H_2 at 300 K, a rapid decrease in the Ir−C coordination number ensued, from ∼4 to ∼2, with the concomitant appearance of a new Ir−light backscatterer contribution at a longer distance having a coordination number of ∼2, assigned to the Ir−C_{long} shell of σ-bonded ethyl ligands (Table S2).

In contrast, when the support was MgO, no change in the Ir−C contribution at the shorter Ir−backscatterer distance was detected, even after H_2 flow for 2 h at 300 K (Table S3). The Ir−C coordination number of ∼4 remained nearly constant, without the appearance of the Ir−C_{long} contribution, indicating that the initially π-bonded ethene ligands were highly stable in the iridium complex on MgO, in agreement with the IR data.

Moreover, the EXAFS data characterizing both the zeolite- and MgO-supported samples in flowing H_2 at 300 K and 1 bar are consistent with the presence of site-isolated mononuclear iridium complexes, as evidenced by the absence of any Ir−Ir contribution (which would be attributed to iridium clusters).

Activities of Supported Iridium Complexes for Catalysis of Ethene Hydrogenation and Isotopic H_2/D_2 Exchange. The zeolite- and MgO-supported iridium complexes after the aforementioned treatments were tested as catalysts for the hydrogenation of ethene and for the isotopic exchange reaction involving H_2 and D_2; data were obtained in an ideal once-through tubular plug-flow reactor at 300 K and 1 bar.

dx.doi.org/10.1021/cs200397r |ACS Catal. 2011, 1, 1549–1561

The data were used to determine initial rates of the catalytic reactions, as described previously.[17] The catalytic results are summarized in Table 1, together with information about the catalyst pretreatment conditions and the corresponding structures elucidated spectroscopically.

In the hydrogenation of ethene, carried out with a feed consisting of H_2 + C_2H_4 in a 2:1 molar ratio, the only product was ethane. The activity of the initially prepared zeolite-supported catalyst (incorporating $Ir(C_2H_4)_2$ complexes) for ethene hydrogenation was measured because the turnover frequency (TOF) was found to be more than 20 times greater than that of the initially prepared MgO-supported iridium complex.

In contrast, each of the zeolite-supported iridium complexes incorporating CO ligands together with C_2H_4 ligands (formed by the treatments indicated in Table 1) was found to be inactive for ethene hydrogenation.

On the other hand, most of the zeolite- and MgO-supported catalysts were active for the HD exchange reaction, as determined in experiments in which equimolar mixtures of H_2, D_2, and C_2H_4 diluted with helium were fed to the flow reactor.[18] The results summarized in Table 1 show activities measured as fractional conversions relative to the equilibrium conversion at 300 K and 1 bar.

As shown in Table 1, the activity for HD exchange of the catalyst initially in the form of the zeolite-supported $Ir(C_2H_4)_2$ was more than an order of magnitude greater than the activities of the zeolite-supported iridium complexes that incorporated CO ligands, and it was also an order of magnitude greater than that of the catalyst that was initially in the form of $Ir(C_2H_4)_2$ species supported on MgO.

DISCUSSION

Structures of Iridium Diethene Complexes Supported on Zeolite HY and on MgO. The results demonstrate that, upon adsorption of $Ir(C_2H_4)_2(acac)$ with removal of the acac ligand, iridium diethene complexes were formed on either highly dealuminated zeolite Y or highly dehydroxylated MgO. These complexes are anchored by Ir−O bonds and, when the support is the zeolite, located at Al sites of the supports; the supports behave as bidentate ligands. These iridium diethene complexes on the supports are isostructural and thus provide ideal starting points into this investigation of ligand effects in catalysis. Thus, by carrying out experiments with isostructural iridium complexes on supports with contrasting properties, we have been able to unravel the effects of the supports and other ligands on the reactivities and catalytic activities of the mononuclear site-isolated iridium complexes. This elucidation of ligand effects is comparable to what is achievable in homogeneous organometallic catalysis, and we emphasize the importance in this research of working with gas-phase reactants and thereby eliminating complicating solvent effects.

We infer that as a consequence of the adsorption on the acidic sites of the zeolite,[19−21] the Ir atoms are more electron-deficient than those in the isostructural complexes on the MgO support.[22] On the basis of electron counting, we postulate that an electron is withdrawn from the Ir atom of the iridium complex as a consequence of the adsorption on the acidic sites of the zeolite. In contrast, the support oxygen atoms on the basic MgO surface are regarded as electron donors. Thus, we infer that the MgO-supported iridium diethene complexes are formally 17-electron species (2 e^- from each ethene ligand, 9 e^- from the Ir atom, and 4 e^- from the two oxygen atoms of the support), and the zeolite-supported iridium diethene complexes are regarded as formally 16-electron species (2 e^- from each ethene ligand, 9 e^- from the Ir atom, and 3 e^- from the two oxygen atoms of the support; note that the aluminum atoms in the framework of the zeolite are regarded as Al^- (with a local negative net charge)). (We stress that these statements are approximate and that the electron counting is just a formalism.) Evidence of our inferences about the effects of the supports as ligands is provided by the frequencies of the carbonyl bands in the $Ir(CO)_2$ complexes discussed in the following section.

As summarized in the following paragraphs, these differences in electron density are associated with profound differences in the reactivity and catalytic activity of the supported iridium complexes.

Reactivities of Mononuclear Iridium Complexes with CO: Influence of the Support. The iridium diethene complexes supported on the zeolite and on MgO were facilely converted into iridium dicarbonyl complexes when exposed to pulses of CO, as evidenced by the IR and EXAFS spectra (Figure 1, Table 1), consistent with previous reports.[4,5] The formation of iridium *gem*-dicarbonyls occurred rapidly on each support, in agreement with the general pattern that group-8 metal carbonyls are more stable than group-8 metal ethene complexes,[23] which is consistent with the relatively high strength of the metal−CO bond.

In comparison with the ν_{CO} frequencies characterizing the $Ir(CO)_2(acac)$ precursor in tetrahydrofuran solution (at 2007 and 2063 cm^{-1}), those characterizing the supported $Ir(CO)_2$ species on the zeolite, at 2038 and 2109 cm^{-1}, are blue-shifted, whereas they are red-shifted when the support is MgO (1967 and 2051 cm^{-1}). As the metal becomes more electron-deficient, the electron density transferred from the CO to the metal through σ donation increases, leading to the strengthening of the C−O bond and, therefore, positive shifts of the ν_{CO} bands. In contrast, when CO is bonded to an electron-rich metal, π back-donation from the metal dominates, which weakens the C−O bond, causing a red shift of the CO frequency.[24] These results demonstrate the contrasting electron−acceptor and electron−donor properties of the two supports, respectively.[25] Thus, the IR data demonstrate the presence of relatively electron-deficient iridium species on the zeolite and electron-rich iridium species on the MgO.

Evidence of the contrasting reactivities of the isostructural iridium complexes on these supports is provided by IR spectra characterizing the samples in CO. The data indicate unusual ligation of the iridium complexes when they are supported on the zeolite, because treatment of this sample with CO led to the appearance of a new band at 2073 cm^{-1}, in addition to the bands indicative of the iridium dicarbonyls at 2038 and 2109 cm^{-1} (Figure S9). In contrast, no new bands different from those ascribed to $Ir(CO)_2$ were observed for the MgO-supported sample.

The presence of the 2073-cm^{-1} band characterizing the zeolite-supported species agrees well with the formation of tricarbonyl iridium species reported by Mihaylov et al.,[11] when Ir^+ was present on acidic zeolites such as HZSM-5. The intensities of the peaks in the spectrum of our sample (Figure S9) indicate that the ratio of iridium tricarbonyls to iridium dicarbonyls is low, with these two complexes present in a mixture and perhaps equilibrated in the presence of gas-phase CO. Consistent with this inference, when the CO flow was stopped and the IR cell was purged with helium, the iridium tricarbonyl band disappeared,

dx.doi.org/10.1021/cs200397r |ACS Catal. 2011, 1, 1549–1561

leaving the iridium *gem*-dicarbonyls as the only supported iridium species.

Reactivity of Zeolite-Supported Iridium Complexes with CO and C_2H_4. The general pattern that transition metals tend to establish strong metal−CO bonds agrees well with our observation that $Ir(CO)_2$ complexes on the surface of MgO are highly stable in a continuous flow of ethene, because the replacement of the CO ligands by C_2H_4 evidently did not occur, even after 2 h of contact with C_2H_4, which is indicated by the lack of significant changes in the IR and EXAFS spectra after 2 h of C_2H_4 flow.

In contrast, the zeolite-supported $Ir(CO)_2$ complexes under the same conditions gave evidence of an intriguing coordination chemistry of the mononuclear iridium complexes on the markedly electron-withdrawing zeolite support. Treatment of the iridium dicarbonyl on the zeolite with C_2H_4 led to a change in the iridium ligation characterized by the disappearance of the two IR bands assigned to $Ir(CO)_2$ species (at 2038 and 2109 cm^{-1}) and the appearance of two new bands, at 2054 and 2087 cm^{-1} (Figure 2). The appearance of the latter bands was accompanied by formation of other bands in the ν_{CH} stretching region, at 3023 and 3078 cm^{-1} (Figure S1), which became evident after purging of the gas-phase ethene with helium. These results are a clear indication of the formation of ethene ligands π-bonded to the iridium sites.

Significantly, the observed frequencies are slightly shifted relative to those of the iridium diethene complex on the acidic zeolite, demonstrating that the ethene ligands on the iridium were present in an environment different from that of the initial iridium diethene complex. Because the spectra demonstrate the presence of some CO ligands remaining on the iridium (Figure 4), we infer that the CO ligands affected the bonding of ethene to the iridium.

The disappearance of the carbonyl bands initially present and indicative of the iridium dicarbonyl when C_2H_4 came in contact with the sample, combined with the appearance of the new band at 2054 cm^{-1}, calls to mind the result observed with DAY-zeolite-supported rhodium complexes treated under essentially the same conditions.[13] The reported IR and EXAFS spectra implied the formation of $Rh(CO)(C_2H_4)$ species, which were confirmed by calculations at the level of density functional theory (DFT). However, in the case of the zeolite-supported iridium complexes, an additional carbonyl band (at 2087 cm^{-1}) was stable when the sample was in flowing C_2H_4, indicating either the existence of a second carbonyl ligand or the presence of two different types of iridium carbonyl complexes.

Evidence of the latter, rather than one type of iridium complex with two CO ligands, is provided by the IR spectra recorded as the sample temperature was ramped up as C_2H_4 flow continued: the peak at 2087 cm^{-1} gradually decreased in intensity, with a concomitant growth of the peak at 2054 cm^{-1} (Figure 3). The total area under the two peaks was nearly constant, suggesting a stoichiometric transformation of one species into others. Moreover, the total area under these peaks was found to be ∼60% of the original area corresponding to the $Ir(CO)_2$ species before the C_2H_4 treatment, suggesting that each Ir atom was bonded to only one CO ligand when the sample was in the alkene stream. Thus, because the IR spectra also indicate the presence of ethene bonded to the iridium centers, we postulate that the two carbonyl bands of the iridium dicarbonyl, at 2054 and 2087 cm^{-1}, are associated with $Ir(CO)(C_2H_4)$ and $Ir(CO)(C_2H_4)_2$, respectively, which we suggest to have been in equilibrium with each other when the sample was in the C_2H_4 stream, with the changing temperature shifting the equilibrium for desorption of the second C_2H_4 ligand, as shown in Figure 3 (inset).

Scheme 1. Structural Changes Occurring in DAY-Zeolite-Supported Iridium Complexes, Initially Present as $Ir(C_2H_4)_2$, When Exposed to Various Gases[a]

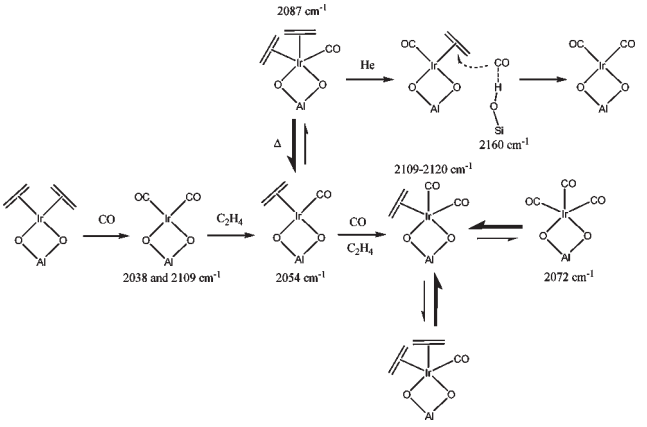

[a] IR frequencies are shown on the scheme.

In agreement with this inference, the band at 2087 cm^{-1}, which appeared at room temperature with the sample in C_2H_4 and which we assign to supported $Ir(CO)(C_2H_4)_2$, gradually disappeared after the C_2H_4 flow was stopped and the cell was purged with helium, which led to a concomitant growth of the band ascribed to $Ir(CO)(C_2H_4)$ species at 2054 cm^{-1} (Figure 4). Moreover, the bands initially present at 2038 and 2109 cm^{-1}, assigned to iridium *gem*-dicarbonyls, were partially recovered during the helium purge. An analysis of the IR spectra indicated that these species may have arisen from small amounts of CO weakly bonded to the nonacidic and acidic hydroxyl groups of the zeolite, consistent with the weak bands observed in the IR spectra at 2160 and 2178 cm^{-1}, respectively;[26,27] these CO molecules are inferred to have migrated to the iridium centers upon removal of the gas-phase products, as indicated by the time-resolved IR spectra shown in Figures 2 and 4 (insets).[28]

Formation of New Zeolite-Supported Iridium Carbonyl Complexes during Competitive Adsorption of CO and C_2H_4. Additional evidence of the new ligand chemistry of the zeolite-supported iridium complexes was provided in experiments characterizing the reactivities of these complexes in flowing mixtures of C_2H_4 and CO. The presence of CO impurities in hydrocarbons, even at low concentrations, often leads to deactivation or poisoning of catalysts by strong adsorption of CO on metal centers, especially at relatively low reaction temperatures. In this situation, the activation of CO by the metal center may prevail over the adsorption of other compounds, such as alkenes, as we observed for iridium complexes supported on MgO (the resulting iridium *gem*-dicarbonyls were shown to be highly stable, with no replacement of the CO ligands by ethene) (Figure S2).

In contrast, contacting of the zeolite-supported iridium complexes with a mixture of ethene and CO resulted in an IR spectrum including bands at 2087 and 2111 cm^{-1} (Figure 5). The frequency of the less intense band at 2087 cm^{-1} exactly matches that of the $Ir(CO)(C_2H_4)_2$ species inferred to have formed upon treatment of the zeolite-supported $Ir(CO)_2$ complexes with C_2H_4 (Figure 2); consequently, we make the same assignment; namely, $Ir(CO)(C_2H_4)_2$.

dx.doi.org/10.1021/cs200397r |ACS Catal. 2011, 1, 1549–1561

On the other hand, we ascribe the 2111-cm^{-1} band to the formation of $Ir(CO)_2(C_2H_4)$ complexes in the presence of CO and C_2H_4 because one of the ethene ligands in $Ir(CO)(C_2H_4)_2$ is facilely replaced by a second carbonyl ligand from the gas phase. This assignment is consistent with the fact that the area under the two peaks represents ~92% of that of the two bands characterizing pure $Ir(CO)_2$ species, a result that indicates that the majority of the iridium species were still bonded to two CO ligands. Furthermore, the presence of $Ir(CO)_2$ and $Ir(CO)_3$ species can be ruled out because of the absence of bands at 2038 and 2073 cm^{-1}, respectively. Thus, our results imply the presence of $Ir(CO)_2(C_2H_4)$ and $Ir(CO)(C_2H_4)_2$ in the presence of gas-phase CO + C_2H_4, highlighting the role of the zeolite in stabilizing electron-deficient iridium complexes that can accommodate an unusually large number of ligands (three labile ligands, including two CO and one C_2H_4, plus the support). The proposed structures of the zeolite-supported iridium complexes resulting from the various treatments are illustrated in Scheme 1.

Confirmation of IR Results by X-ray Absorption Spectra. A comparison of the Fourier transforms of the EXAFS data characterizing each form of the catalyst is provided in Figure 6. The magnitude of the EXAFS (χ) function at ~2.4 Å (the distance is not corrected for phase shifts), assigned to $Ir-O_{CO}$ contributions, matches our interpretation of the IR results as follows: The $Ir-O_{CO}$ contribution is shown to be relatively large and similar for spectra b and c (corresponding to $Ir(CO)_2$ and $Ir(CO)_2(C_2H_4)$ species, respectively, according to our IR analysis), but it is much less for spectra d and e (assigned to $Ir(CO)(C_2H_4)$ species), and it is almost nonexistent for spectrum a, representing only $Ir(C_2H_4)_2$ species (a residual contribution can be still observed, resulting from the interaction between the Ir atoms and the support at the Al sites, the Ir−Al contribution).

We emphasize that we attempted to include Ir−Ir contributions in each of the fits, but no models including these contributions were found at any of the tested *k*-weightings to give nearly satisfactory overall fits or appropriate goodness of fit values. This result, combined with the IR results showing sharp peaks in the ν_{CO} region assigned to the mononuclear iridium carbonyl complexes and the absence of bridging carbonyl bands (characterized by frequencies less than 2000 cm^{-1}),[29] indicates that there was no detectable iridium cluster formation under our conditions and that the mononuclear iridium complexes were stable.

The XANES data show no observable shifts in the edge energy of the iridium in the supported complexes as a result of treatments with various mixtures of CO and C_2H_4, which is consistent with the suggestion that the formal oxidation state of the iridium did not change enough for us to observe. This result is consistent with the inference that CO and C_2H_4 ligands do not substantially modify the oxidation state of the iridium in the supported iridium complex.[30]

Nonetheless, the XANES region of each spectrum gives evidence of changes in the ligation of iridium in the various reactive atmospheres (Figure 7). Strong similarities are evident between the spectrum taken after injection of a pulse of CO into the cell with a sample initially incorporating $Ir(C_2H_4)_2$ complexes and that taken with the sample in a mixture of CO + C_2H_4 (spectra b and c), both corresponding to iridium species bonded to two CO ligands, as shown by the IR data. A similar comparison can be made for spectra d and e of Figure 7, corresponding to the XANES region of samples consisting primarily of supported complexes with only one CO ligand. These are similar to each other but notably different from those represented by spectra b and c. Furthermore, the XANES regions of spectra b, c, d, and e (representing iridium complexes with one or two CO ligands) are markedly different from those of spectrum a (representing iridium complexes with no CO ligands), which is consistent with the quantitative analysis of the EXAFS data (Table 1) and with the analysis of the corresponding IR spectra.

The XANES spectra characterizing the samples resulting from the various treatments are not characterized by well-defined isosbestic points (Figure 7, inset), a result that indicates that the corresponding iridium complexes are intermediates in the transformations rather than unique species formed in stoichiometrically simple reactions of the initial species.[31]

In summary, the XANES data point to mixtures containing more than two supported species.[32] This observation is consistent with the inference that $Ir(CO)(C_2H_4)$, $Ir(CO)_2(C_2H_4)$, and $Ir(CO)(C_2H_4)_2$ are intermediates in the transformation of $Ir(C_2H_4)_2$ into $Ir(CO)_2$.

Activation of π-Bonded Ethene Ligands and Reactivity of Supported Iridium Complexes with H_2: Implications Regarding Support and Ligand Effects in Catalysis by Metal Complexes. The data characterizing the ligand chemistry of the mononuclear iridium complexes on supports with markedly different properties, the electron-donating MgO and the electron-withdrawing DAY zeolite, show that the reactivity of the iridium species for bonding to molecules from the gas phase can be tuned by the choice of the support acting as a macroligand; there is a clear analogy with the roles of ligands in organometallic solution chemistry.[30]

The data demonstrate that the tendency of the iridium complexes to bond to ligands such as alkenes is markedly enhanced by the zeolite, because as a ligand, this support is responsible for the generation of electron-deficient iridium sites that can accommodate a relatively large number of ligands. This intriguing role of the acidic support makes it possible to activate various reactive groups simultaneously, which is often a necessary (although often not sufficient) criterion for catalysis of reactions involving more than one reactant (we recognize that there are exceptions, such as reactions proceeding via Eley−Rideal mechanisms, whereby one of the reactants is bonded to the catalyst and the other reacts directly from the fluid phase). A recent investigation[33] showed, on the basis of time-resolved IR and EXAFS data, that hydrogenation of the initially present iridium ethylene complex on the zeolite support can be attributed to its ability to simultaneously activate both ethene and H_2, in contrast to the reactivity of the isostructural iridium complex on MgO.

The reactivity of the zeolite-supported iridium complexes implies that new bonds can be formed facilely with the reactants from the fluid phase because the metal can share a larger number of electrons with those reactants than when the support is MgO; this reactivity has important implications for catalysis.

Indeed, our catalytic experiments characterizing the isotopic exchange in the reaction of H_2 with D_2 show that the reactivity of the mononuclear iridium complexes with H_2 is strongly dependent on the electron-withdrawing or electron-donating properties of the support (Table 1). Evidence of the effect is provided by a comparison of the activity of the isostructural MgO- and zeolite-supported $Ir(C_2H_4)_2$ complexes for the activation of H_2, as indicated by the results of the H_2 + D_2 reaction experiments: the reaction takes place much faster when the support is the zeolite rather than MgO.

dx.doi.org/10.1021/cs200397r |*ACS Catal.* 2011, 1, 1549–1561

In agreement with the results of the H_2 + D_2 exchange experiments, the stability of the C═C bond in the $Ir(C_2H_4)_2$ complexes was shown to be high when the iridium was supported on MgO, in contrast to the results observed with the electron-deficient iridium species on the zeolite, for which the ethene ligands were rapidly transformed into ethyl, forming $Ir(C_2H_5)_2$ species, as evidenced by IR and EXAFS spectra (Figure S1, Table S2, respectively).

Consistent with the reactivities of these two catalysts for H_2 dissociation and the reactivity of the C═C group in site-isolated iridium complexes, the catalyst initially consisting of zeolite-supported $Ir(C_2H_4)_2$ species is evidently much more active than the comparable MgO-supported catalyst for the ethene hydrogenation (Table 1).

On the other hand, we also evaluated the catalytic performance of the zeolite-supported iridium complexes when they initially incorporated different combinations of C_2H_4 and CO ligands; the inferences were drawn on the basis of the structures elucidated from IR and EXAFS data characterizing the samples, in contact with the various reaction mixtures. When the iridium complexes incorporated both CO and ethene ligands, the stability of ethene bonded to the iridium was markedly higher than in the $Ir(C_2H_4)_2$ complex, as demonstrated by the IR spectra of the sample in H_2 at 300 K for 1 h (compare Figure S3, characterizing $Ir(C_2H_4)_2$ species, with Figure S4, characterizing $Ir(CO)(C_2H_4)$). In contrast to the spectra of the $Ir(C_2H_4)_2$ complexes on the same acidic support, the ν_{CH} stretching region of the spectrum shows that the π-bonded ethene ligands were highly stable in the presence of H_2 (note that the band at 3023 cm^{-1} was partially shifted to 3012 cm^{-1}, possibly because of a slight change in the electronic environment of the iridium while the H_2 activation was occurring).

The reactivity for H_2 dissociation of each of the CO-containing iridium complexes supported on the zeolite was found to be rather low relative to that of $Ir(C_2H_4)_2$ on the same support, and the former complexes are characterized by catalytic performance similar to that representative of the samples initially consisting of $Ir(C_2H_4)_2$ on MgO. However, the former class of catalysts appeared to be completely inactive for ethene hydrogenation, whereas the latter was active for this reaction, with an intermediate reaction rate by the standards of our samples (Table 1).

Although $Ir(CO)_2$ complexes supported on MgO did not evidence any reactivity for the dissociation of H_2, the isostructural complexes on the zeolite were found to be moderately active as H_2 dissociation catalysts, with an activity similar to that observed for samples initially consisting of $Ir(C_2H_4)_2$ complexes on the basic MgO support. This result indicates, once more, the importance of the support as a ligand anchoring the iridium sites. Hence, the samples initially consisting of $Ir(C_2H_4)_2$ and of $Ir(CO)_2$ complexes supported on the zeolite are more reactive for H_2 dissociation and more active catalytically for ethene hydrogenation, and the ligands are more reactive than those in the isostructural complexes supported on MgO (Table 1).

In summary, the ethene hydrogenation and HD exchange catalysis data (Table 1) indicate that the activity of the mononuclear supported iridium complexes for the dissociation of H_2 is reduced as (a) the zeolite support is replaced by MgO, (b) the total number of ligands on the iridium is increased, and (c) the number of CO ligands on the iridium is increased.

On the basis of our results, we can begin to elucidate how the support and other ligands affect the catalytic performance during the hydrogenation of alkenes: when $Ir(C_2H_4)_2$ complexes are present on the surface of the zeolite, H_2 dissociation is fast, and as a result, the two ethene ligands are highly labile and can be partially hydrogenated rapidly in the presence of H_2, leading to the formation of $Ir(C_2H_5)_2$. Subsequently, the ethyl ligands are rapidly converted to ethane and desorb via reductive elimination. In the cases of (a) the $Ir(C_2H_4)_2$ on MgO and (b) $Ir(CO)(C_2H_4)$ and $Ir(CO)(C_2H_4)_2$ on the zeolite, the ethene ligands are much less reactive in the presence of H_2 as a consequence of the electron-donating character of MgO and the effect of the CO ligands, respectively, causing the complexes to be poorly active, or even completely inactive, for dissociation of H_2. The subsequent steps leading to the conversion of ethene to ethyl and the conversion of ethyl to ethane are relatively slow on these latter catalysts.

CONCLUSIONS

A site-isolated iridium complex incorporating two ethylene ligands was anchored to the surfaces of dealuminated HY zeolite and highly dehydroxylated MgO, resulting in isostructural $Ir(C_2H_4)_2$ complexes differing only in the support, which acts in each case as a bidentate ligand. The interaction of the iridium complexes with various mixtures of H_2, CO, and C_2H_4 were characterized by IR, XANES, and EXAFS spectroscopies. The catalytic activities for ethene hydrogenation and H_2/D_2 exchange reactions were also measured. The data indicate that the zeolite-supported iridium complexes are more electron-deficient than the comparable MgO-supported iridium complexes. As a result, the zeolite-supported iridium complexes are capable of bonding to more ligands than the MgO-supported complexes and are more active as catalysts. The results demonstrate the role of supports as ligands, which directly influence the reactivity and catalytic activity of the supported species. The opportunity to tune the properties of supported catalysts by modifying the support is critical for the design of more efficient supported catalysts.

EXPERIMENTAL METHODS AND DATA ANALYSIS

Materials and Sample Preparation. Sample synthesis and handling were performed with the exclusion of moisture and air. H_2 was supplied by Airgas (99.999%) and was purified by passage through traps containing reduced particles of Cu/Al_2O_3 and activated zeolite 4A to remove traces of O_2 and moisture, respectively. Helium (Airgas, 99.999%) and C_2H_4 (Airgas, 99.99%) were purified by passage through similar traps. CO (Matheson, 99.999%) in a 10% mixture with helium was purified by passage through a trap containing activated γ-Al_2O_3 particles and zeolite 4A to remove any traces of metal carbonyls (from high-pressure gas cylinders) and moisture, respectively. D_2 (99.8%) was purchased from Cambridge Isotope Laboratories. The highly dealuminated HY zeolite (DAY Zeolite; Zeolyst International, CBV760), with a Si/Al atomic ratio of ~30, was calcined in O_2 at 773 K for 4 h and was evacuated for 16 h at 773 K. MgO (EM Science; surface area is approximately 100 m^2/g) was mixed with deionized water to form a paste, which was dried overnight in air at 393 K. The resultant solid was ground and treated in O_2 as the temperature was ramped linearly from room temperature to 973 K and then held for 2 h, resulting in a high degree of dehydroxylation.[7] After calcination, the zeolite and the MgO were isolated, and each was stored in an argon-filled glovebox (MBraun, with an H_2O level less than 0.5 ppm and an O_2 level less than 5 ppm) until use. *n*-Pentane solvent (Fisher, 99%) was

dx.doi.org/10.1021/cs200397r |ACS Catal. 2011, 1, 1549–1561

dried and purified by column chromatography (Grubbs apparatus, MBraun SPS) in the presence of argon.

The precursor $Ir(C_2H_4)_2(acac)$ (acac = $CH_3COCHCOCH_3$) was synthesized as described elsewhere;[6] it has been characterized by X-ray diffraction crystallography and ^1H and ^{13}C NMR, Raman, and IR spectroscopies. To prepare the supported iridium complex, $Ir(C_2H_4)_2(acac)$ and the calcined zeolite or MgO powder in a Schlenk flask were slurried in dried *n*-pentane that was initially at ice temperature. The stirred slurry was warmed to room temperature, and after 1 day, the solvent was removed by evacuation for 1 day so that all the iridium remained on the support. The resultant solids, each containing 1 wt % Ir, were stored in the argon-filled glovebox.

IR Spectroscopy. A Bruker IFS 66v/S spectrometer with a spectral resolution of 2 cm^{-1} was used to collect transmission IR spectra of powder samples. Approximately 30 mg of solid sample in a glovebox was pressed into a thin wafer and loaded into a cell that served as a flow reactor (In-situ Research Institute, Inc., South Bend, IN). The cell was sealed and connected to a flow system that allowed recording of spectra as the reactant gases flowed through the cell at reaction temperature. Each reported spectrum is the average of 64 scans.

Ethene Hydrogenation Catalysis in a Flow Reactor. Ethene hydrogenation catalysis was carried out in a conventional laboratory once-through tubular plug-flow reactor. The catalyst (30 mg of zeolite-supported catalyst or 150 mg of MgO-supported catalyst) was diluted with 10 g of inert, nonporous α-Al_2O_3 and loaded into the reactor in a glovebox. In the reaction experiments, the feed C_2H_4 and H_2 partial pressures were 333 and 666 mbar, respectively, with the balance being helium; the feed flow rate was 60 mL/min, and the total pressure, atmospheric. The reactor temperature was 300 ± 1 K.

Products were analyzed by gas chromatography with an HP-6890 instrument equipped with a 50 m × 0.53 mm PLOT Alumina "M" capillary column (J & W Scientific) and a flame-ionization detector. The product stream from the reactor was sampled every 12 min and analyzed. The ethene conversions were <5%, and the reactor was approximated as differential. Slow catalyst deactivation was observed during reaction, probably because of the formation of small amounts of heavier hydrocarbons, as evidenced by mass spectra of the products; these heavier hydrocarbons could poison the metal species by irreversible adsorption or they could form coke. To eliminate the effect of the deactivation, the activity of each catalyst was extrapolated to time on stream (TOS) = 0 from the corresponding TOF vs TOS plots. At these low TOS values, the only observed reaction product was ethane.

H_2/D_2 Exchange Experiments. The catalyst (30 mg) was diluted with 5 g of inert, nonporous α-Al_2O_3 and loaded into the reactor in a glovebox. The feed C_2H_4, H_2, and D_2 partial pressures were each 200 mbar, with the balance being helium; the total feed flow rate was 100 mL/min, and the total pressure, atmospheric. The reactor temperature was 300 ± 1 K, controlled with water in a cooling jacket. Mass spectra of the gases introduced into the flow system and the effluents produced by reaction were measured with an online Balzers OmniStar mass spectrometer running in multi-ion monitoring mode. Changes in the signal intensities of H_2 (m/z = 2), D_2 (m/z = 4), HD (m/z = 3), CO (m/z = 28), C_2H_4 (m/z = 26, 27, and 28), C_2H_6 (m/z = 26, 27, 28, and 30), C_4H_8 (m/z = 41 and 55), and C_4H_{10} (m/z = 43 and 56) were recorded. The reported intensity values were corrected by subtracting background intensities recorded as the reactant gas mixture bypassed the flow reactor containing the catalyst. The HD exchange was measured at room temperature for times on stream <10 min, for which the nuclearity of the iridium complexes initially present as single-atom complexes was maintained, as demonstrated by IR and EXAFS spectroscopy. We emphasize that the amount of H_2 and D_2 consumed in the formation of ethane was, under the selected conditions, negligible with respect to the HD exchange.

X-ray Absorption Spectroscopy. The X-ray absorption spectra were recorded at X-ray beamline 4−1 at the Stanford Synchrotron Radiation Lightsource (SSRL). The storage ring electron energy and ring current were 3 GeV and 300 mA, respectively. A double-crystal Si(220) monochromator was detuned by 20−25% at the Ir L_{III} edge to minimize effects of higher harmonics in the X-ray beam.

In an N_2-filled glovebox at SSRL, each powder sample was loaded into a cell that served as a flow reactor,[34] which was sealed in the inert atmosphere. The mass of each sample (~0.3 g) was chosen for optimal absorption measurements at the Ir L_{III} edge (11 215 eV, giving an X-ray absorbance of approximately ~2.0 calculated at an energy 50 eV greater than the absorption edge). Spectra were collected in transmission mode with the presence of flowing gases at 1 bar and at temperatures between 300 and 393 K. Data were recorded for 15 min to determine each spectrum.

EXAFS Data Analysis. The X-ray absorption edge energy was calibrated with the measured signal of a platinum foil (scanned simultaneously with the sample) at the Pt L_{III} edge, which was taken to be the inflection point at 11 564 eV. The data were normalized by dividing the absorption intensity by the height of the absorption edge.

Analysis of the EXAFS data was carried out with ATHENA of the software package IFEFFIT[35,36] and with the software XDAP developed by Vaarkamp et al.[37] Each spectrum that was subjected to analysis was the average of 2−4 consecutively recorded spectra. ATHENA was used for edge calibration, deglitching, and data normalization. XDAP was used for background removal, normalization, and conversion of the data into an EXAFS (χ) file. A "difference file" technique was applied with XDAP for determination of optimized fit parameters. Each spectrum was processed by fitting a second-order polynomial to the pre-edge region and subtracting this from the entire spectrum. The functional that was minimized and the function used to model the data are presented elsewhere.[38] The background was subtracted by using cubic spline routines. Reference backscattering phase shifts were calculated from crystallographic data with the software FEFF7.[39] As references, $Ir(C_2H_4)_2(acac)$[6] was used for $Ir-O_{zeolite}$, $Ir-O_{MgO}$, Ir−C, and $Ir-C_{long}$ contributions; $Ir(CO)_2(acac)$[40] was used for $Ir-C_{CO}$ and $Ir-O_{CO}$ contributions for the Ir−CO shell, which is characterized by the multiple scattering that is representative of linear Ir−C−O moieties.[41,42] Ir−Al alloy[43] was used for the Ir−Al contribution; Ir−Mg alloy[43] was used for the Ir−Mg contribution; and iridium metal[43] was used for the Ir−Ir contribution. These contributions were selected for EXAFS analysis because they were all expected on the basis of reports of EXAFS spectroscopy of similar supported organometallic complexes.[4,12,44]

The number of parameters used in the fitting was always less than the statistically justified number, computed with the Nyquist theorem:[45] $n = (2\Delta k \Delta r/\pi) + 1$, where Δk and Δr, respectively, are the k and r ranges used in the fitting.

In the development of best-fit models of each of the EXAFS data, various combinations of plausible absorber-backscatterer contributions were fitted initially, which led to a list of candidate models narrowed on the basis of the goodness of fit and the

dx.doi.org/10.1021/cs200397r |ACS Catal. 2011, 1, 1549–1561

overall fit in both k and R space. Then, a "difference-file" technique was applied to the candidate models, whereby the calculated EXAFS contribution from each individual Ir−backscatterer contribution was compared with the data in R space (calculated by subtracting all the other calculated Ir−backscatterer contributions from the experimental overall contributions). This iterative fitting was continued in R space of both overall and individual contributions with the Fourier-transformed χ data until the best-fit model was obtained, which is the one providing optimum agreement between the calculated k^0-, k^1-, k^2-, and k^3-weighted EXAFS data and the model.

When iridium is bonded to both CO and C_2H_4 ligands, EXAFS data are not sufficient to distinguish the Ir−backscatterer contributions from Ir−support oxygen contributions and Ir−C contributions expected for iridium complexes with ethene ligands. However, it has been shown in previous investigations that similar zeolite-supported complexes of group-8 metals are strongly bonded to the support through two metal−oxygen bonds.[4,12,44] Indeed, our EXAFS data show that the supported $Ir(C_2H_4)_2$ and $Ir(CO)_2$, initially bonded to the zeolite by two Ir−O bonds at Al^- sites, retained an Ir−Al coordination number of ∼1 throughout all the treatments, indicating that the iridium−support bonding was stable. The inference that the iridium complexes remain bonded at the aluminum sites in the zeolite is consistent with the observed extraordinary ligation properties, discussed above. Therefore, we infer that each iridium complex remained bonded to two support oxygen atoms under all the treatment conditions.

On the basis of these inferences, we can tentatively estimate the coordination number for $Ir-C_{ethene}$ contributions for each treatment condition (e.g., a total coordination number of 5 for $Ir-O_{zeolite}$ and $Ir-C_{ethene}$ implies the coordination numbers for $Ir-O_{zeolite}$ and $Ir-C_{ethene}$ are 2 and 3, respectively), and the results agree well with the assignments of the iridium species based on our IR data.

■ ASSOCIATED CONTENT

Supporting Information. Additional IR and EXAFS spectra and details of EXAFS analysis are included. This material is available free of charge via the Internet at http://pubs.acs.org.

■ AUTHOR INFORMATION

Corresponding Author

*Phone: (530)752-3953. E-mail: bcgates@ucdavis.edu.

■ ACKNOWLEDGMENT

This research was supported by the DOE (Basic Energy Sciences, Contract FG02-04ER15513) (J.L.). The research received funding from the European Union Seventh Framework Programme (FP7/2007-2013) under grant agreement PIOF-GA-2009-253129 (P.S.). We acknowledge beam time and the support of the DOE Division of Materials Sciences for its role in the operation and development of beamline 4-1 at the Stanford Synchrotron Radiation Lightsource (SSRL). We thank the beamline staff for valuable support.

■ REFERENCES

(1) Coq, B.; Figueras, F. *Cood. Chem. Rev.* **1998**, *178−180*, 1753.
(2) Kawi, S.; Gates, B. C. In *Clusters and Colloids: From Theory to Applications*; Schmid, G., Ed.; VCH: New York, 1994; p 299−365.
(3) Goellner, J. F.; Gates, B. C.; Vayssilov, G. N.; Rösch, N. *J. Am. Chem. Soc.* **2000**, *122*, 8056–8066.
(4) Uzun, A.; Bhirud, V. A.; Kletnieks, P. W.; Haw, J. F.; Gates, B. C. J. *Phys. Chem. C* **2007**, *111*, 15064–15073.
(5) Uzun, A.; Ortalan, V.; Browning, N. D.; Gates, B. C. *Chem. Commun.* **2009**, *31*, 4657–4659.
(6) Bhirud, V. A.; Uzun, A.; Kletnieks, P. W.; Craciun, R.; Haw, J. M.; Dixon, D. A.; Olmstead, M. M.; Gates, B. C. *J. Organomet. Chem.* **2007**, *692*, 2107–2113.
(7) Niu, H.; Yang, Q.; Tang, K.; Xie, Y. *Microporous Mesoporous Mater.* **2006**, *96*, 428–433.
(8) Uzun, A.; Ortalan, V.; Browning, N. D.; Gates, B. C. *J. Catal.* **2010**, *269*, 318–328.
(9) Burkhardt, I.; Gutschick, D.; Landsmesser, H.; Miessner, H. In *Zeolite Chemistry and Catalysis*; Jacobs, P.A., Ed.; Elsevier: Amsterdam, 1991; p 215−222.
(10) Solymosi, F.; Novak, E.; Molnar, A. *J. Phys. Chem.* **1990**, *94*, 7250–7255.
(11) Mihaylov, M.; Ivanova, E.; Thibault-Starzyk, F.; Daturi, M.; Dimitrov, L.; Hadjiivanov, K. I. *J. Phys. Chem. B* **2006**, *110*, 10383–10389.
(12) Liang, A. J.; Bhirud, V. A.; Ehresmann, J. O.; Kletnieks, P. W.; Haw, J. F.; Gates, B. C. *J. Phys. Chem. B* **2005**, *109*, 24236–24243.
(13) Liang, A. J.; Craciun, R.; Chen, M.; Kelly, T. G.; Kletnieks, P. W.; Haw, J. F.; Dixon, D. A.; Gates, B. C. *J. Am. Chem. Soc.* **2009**, *131*, 8460–8473.
(14) Ogino, I.; Gates, B. C. *J. Phys. Chem. C* **2010**, *114*, 8405–8413.
(15) Miessner, H.; Burkhardt, I.; Gutschick, D.; Zecchina, A.; Morterra, C.; Spoto, G. *J. Chem. Soc., Faraday Trans* **1989**, *85*, 2113–2126.
(16) The limitations of the EXAFS analysis when there are so many contributions make it impossible to resolve them all ($Ir-O_{zeolite}$, $Ir-C_{ethene}$, $Ir-C_{CO}$, $Ir-O_{CO}$, and Ir−Al). Because of the similarities between the $Ir-O_{zeolite}$ and $Ir-C_{ethene}$ contributions (in terms of both the atomic weights and bonding distances), we chose for simplicity to lump these two contributions. For details of EXAFS analysis of supported metal complexes, see: Alexeev, O.; Gates, B. C. *Top. Catal.* **2000**, *10*, 273–293.
(17) Serna, P.; Gates, B. C. *J. Am. Chem. Soc.* **2011**, *133*, 4714–4717.
(18) The rates of HD exchange catalyzed by samples initially in the form of $Ir(CO)_2$ or $Ir(C_2H_4)(CO)$ were measured in the absence of C_2H_4 (the H_2/D_2 molar ratio was 1.0), because in the presence of C_2H_4, both complexes were unstable and converted into $Ir(C_2H_4)_2(CO)$ complexes.
(19) Beaumont, R; Barthomeuf, D. *J. Catal.* **1972**, *26*, 218–225.
(20) Beaumont, R; Barthomeuf, D. *J. Catal.* **1972**, *27*, 45–51.
(21) Miessner, H.; Kosslick, H.; Lohse, U.; Parlitz, B.; Tuan, V.-A. *J. Phys. Chem.* **1993**, *97*, 974–9748.
(22) Samant, M. G.; Boudart, M. *J. Phys. Chem.* **1991**, *95*, 4070–4074.
(23) Grunes, J.; Zhu, J.; Yang, M.; Somorjai, G. A. *Catal. Lett.* **2003**, *86*, 15–161.
(24) Hadjiivanov, K. I.; Vayssilov, G. N. *Adv. Catal.* **2002**, *47*, 308–511.
(25) Cotton, F. A.; Wilkinson, G. *Advanced Inorganic Chemistry*; Wiley-Interscience, New York, 1967.
(26) Kondo, J. N.; Domen, K.; Hirose, C. *J. Phys. Chem.* **1995**, *99*, 10573–10580.
(27) Knodo, J. N.; Nishitani, R.; Yoda, E.; Yokoi, T.; Tatsumi, T.; Domen, K. *Phys. Chem. Chem. Phys.* **2010**, *12*, 11576–11586.
(28) We suggest that the removed CO molecules were first adsorbed on the acidic hydroxyl groups on the zeolite and then migrated to the nonacidic hydroxyl groups, with the driving force for the reaction including the interaction between ethene and acidic hydroxyl groups (Figure S8).
(29) Li, F.; Gates, B. C. *J. Phys. Chem. B* **2004**, *108*, 11259–11264.
(30) Astruc, D. *Organometallic Chemistry and Catalysis*; Springer: Berlin, Heidelberg, New York, 2007.

(31) Wang, Q.; Hanson, J. C.; Frenkel, A. I. *J. Chem. Phys.* **2008**, *129*, 234502–234507.
(32) Senior, W. A.; Verrall, R. E. *J. Phys. Chem.* **1969**, *73*, 4242–4249.
(33) Lu, J.; Serna, P.; Aydin, C.; Browning, N. D.; Gates, B. C. J. *Am. Chem. Soc.* **2011**, *133*; DOI: 10.1021/ja206486j.
(34) Odzak, J. F.; Argo, A. M.; Lai, F. S.; Gates, B. C. *Rev. Sci. Instrum.* **2001**, *72*, 3943–3945.
(35) Newville, M.; Ravel, B.; Haskel, D.; Rehr, J. J.; Stern, E. A.; Yacoby, Y. *Physica B* **1995**, *208/209*, 154–156.
(36) Newville, M. *J. Synchrotron Radiat.* **2001**, *8*, 96–100.
(37) Vaarkamp, M.; Linders, J. C.; Koningsberger, D. C. *Physica B* **1995**, *209*, 159–160.
(38) Koningsberger, D. C.; Mojet, B. L.; van Dorssen, G. E.; Ramaker, D. E. *Top. Catal.* **2000**, *10*, 143–155.
(39) Zabinsky, S. E.; Rehr, J. J.; Ankudinov, A.; Albers, R. C.; Eller, M. J. *Phys. Rev. B.* **1995**, *52*, 2995–3009.
(40) Carney, G. O., Jr. Ph.D. Thesis, University of North Carolina at Chapel Hill, 1942.
(41) van Zon, F. B. M.; Kirlin, P. S.; Gates, B. C.; Koningsberger, D. C. *J. Phys. Chem.* **1989**, *93*, 2218–2222.
(42) Duivenvoorden, F. B. M.; Koningsberger, D. C.; Uh, Y. S.; Gates, B. C. *J. Am. Chem. Soc.* **1986**, *108*, 6254–6262.
(43) Pearson, W. B.; Calvert, L. D.; Villars, P. *Pearson's Handbook of Crystallographic Data for Intermetallic Phases*; American Society for Metals: Metals Park, OH, 1985.
(44) Ogino, I.; Gates, B. C. *J. Am. Chem. Soc.* **2008**, *130*, 13338–13346.
(45) Lytle, F. W.; Sayers, D. E.; Stern, E. A. *Physica B* **1989**, *158*, 701–722.